Analytical Letters

ISSN: 0003-2719 (Print) 1532-236X (Online) Journal homepage: http://www.tandfonline.com/loi/lanl20

# Preparation and Spectroscopic, Microscopic, Thermogravimetric, and Electrochemical Characterization of Silver-Doped Cerium(IV) Oxide Nanoparticles

A. A. Ansari, J. P. Labis, M. Alam, Shahid M. Ramay, N. Ahmed & Asif Mahmood

**To cite this article:** A. A. Ansari, J. P. Labis, M. Alam, Shahid M. Ramay, N. Ahmed & Asif Mahmood (2017) Preparation and Spectroscopic, Microscopic, Thermogravimetric, and Electrochemical Characterization of Silver-Doped Cerium(IV) Oxide Nanoparticles, Analytical Letters, 50:8, 1360-1371, DOI: 10.1080/00032719.2016.1218499

**To link to this article:** http://dx.doi.org/10.1080/00032719.2016.1218499

Accepted author version posted online: 24 Jan 2017.
Published online: 24 Jan 2017.

ANALYTICAL LETTERS
2017, VOL. 50, NO. 8, 1360–1371
https://doi.org/10.1080/00032719.2016.1218499

Taylor & Francis
Taylor & Francis Group

NANOTECHNOLOGY



# Preparation and Spectroscopic, Microscopic, Thermogravimetric, and Electrochemical Characterization of Silver-Doped Cerium(IV) Oxide Nanoparticles

A. A. Ansari[a], J. P. Labis[a], M. Alam[b], Shahid M. Ramay[c], N. Ahmed[b], and Asif Mahmood[d]

[a]King Abdullah Institute for Nanotechnology, King Saud University, Riyadh, Kingdom of Saudi Arabia; [b]Research Center, College of Science, King Saud University, Riyadh, Kingdom of Saudi Arabia; [c]Department of Physics, King Saud University, Riyadh, Kingdom of Saudi Arabia; [d]Department of Chemical Engineering, College of Engineering, King Saud University, Riyadh, Kingdom of Saudi Arabia

**ABSTRACT**

Silver ion-doped cerium oxide nanoparticles were prepared by polyol-based coprecipitation. Here, the impact of silver doping is evaluated on the crystallographic, optoelectronic, thermogravimetric, and redox behavior of cerium oxide nanoparticles. Spectroscopic techniques were used to characterize the phase purity, crystallinity, morphological structure, and optical and redox properties of nanoproducts. X-ray diffraction confirmed the formation of well-crystallized cerium oxide tetragonal fluorite. The optical absorption spectra and band gap energy were significantly affected following doping that was influenced by the crystalline size. Temperature production reduction investigated the influence of silver concentration on the redox properties of cerium oxide nanoparticles. These catalysts were reversible in cyclic redox reaction to 500°C, nonpyrophoric, and therefore demonstrated potential for applications for hydrogen generation for fuel cells and electrochemical biosensors.

**ARTICLE HISTORY**
Received 16 June 2016
Accepted 27 July 2016

**KEYWORDS**
Band gap energy; optical properties; silver ion-doped cerium oxide nanoparticles; temperature program reduction



## Introduction

Recently, cerium oxide has received considerable attention due to several advantages in applications that include electrolytes in solid oxide fuel cells (Banerjee et al. 2007; Robert et al. 2007; Yu et al. 2010), humidity sensors, biosensors (Liao et al. 2008), ultraviolet absorbents (Si et al. 2005; Yu et al. 2005), chemical polishing, automotive catalytic converters (Ayastuy et al. 2012; Chang et al. 2012), biomedical science (Chen et al. 2006), and electrochemical biosensors (Ansari et al. 2008; Ansari, Solanki, and Malhotra 2008, 2009). Unique properties of cerium oxide nanoparticles include a blueshift in the ultraviolet absorption spectrum and shifting and broadening in Raman allowed modes with lattice expansion (Deshpande et al. 2005; Wang, Quan, and Lin 2007; Katelnikovas et al. 2008). Moreover, cerium oxide absorbs and releases oxygen that plays a critical role in the overall performance of catalytic activity of cerium oxide. In general, cerium ion exists as $Ce^{3+}$ and $Ce^{4+}$ that depend on the partial pressure of oxygen in their surrounding environment (Deshpande et al. 2005; Wang, Quan, and Lin 2007). In addition, cerium oxide is considered to be a green and inexpensive rare earth oxide for catalysis (Liao et al. 2008).

**CONTACT** A. A. Ansari aneesaansari@gmail.com; amustaqeemahmad@ksu.edu.sa King Abdullah Institute for Nanotechnology, King Saud University, Riyadh 11451, Kingdom of Saudi Arabia.
Color versions of one or more of the figures in the article can be found online at www.tandfonline.com/lanl.

These distinctive characters of cerium oxide nanoparticles are to be beneficial in the present applications and may open new avenues in material science.

Recently, more efforts have tailored catalytic properties of cerium oxide by adding transition metal ions to increase thermal stability, optoelectronic, and electrical properties. Consequently, these novel materials have been used as passive counterelectrodes, solid oxide fuel cells, and electrochemical sensors (Ansari, Solanki, and Malhotra 2008, 2009; Katelnikovas et al. 2008). The ionic conductivity of cerium oxide nanoparticles is affected by the size of dopants (Deshpande et al. 2005) because conductivity is enhanced if the disparity in ionic sizes of host and dopant cations is as low as possible (Si et al. 2005; Yu et al. 2005; Robert et al. 2007; Liao et al. 2008; Yu et al. 2010). Moreover, it was shown that the activation energy of $O^{2-}$ migration for codoped samples with 5 or 10 different dopants was lowered, whereas the ionic conductivity was 30% higher compared to best single doped samples with the same vacancy concentration.

Previously, some researchers investigated the doping of transition metal ions in cerium oxide lattice that greatly enhanced the electrocatalytic performance of cerium oxide nanomaterials (Mitrovic et al. 2007; Ansari, Solanki, and Malhotra 2008; Cai et al. 2014; Zhang et al. 2015). Furthermore, the electrochemical behavior of cerium oxide depends on its crystal structure and surface properties, the specific surface area, pore volume, and pore dimension and distribution. Many efforts considered the synthesis of transition metal ion-doped cerium oxide with controllable morphology and pore structure (Mitrovic et al. 2007; Cai et al. 2014).

To date, many synthesis techniques have been used for the preparation of transition metal ion-doped cerium oxide nanoparticles that include sol–gel, hydrothermal/solvothermal, microwave, combustion, microemulsion, coprecipitation, and complexing route protocols. The complexing route, hydrothermal precipitation, and coprecipitation methods from salt solutions are the frequently used methods due to their high benefit-to-cost ratios (Souza and Muccillo 2009; Wadhwa et al. 2013; NaeemUllah et al. 2014). These methods involve simultaneous nucleation, growth, coarsening, and agglomeration. However, these methods differ according to the preparation parameters. The addition of a low dielectric constant medium to aqueous solution, for example, may alter the kinetics of nucleation and growth of particles (Souza and Muccillo 2009) that may result into changes in the crystallite size and particle size distribution.

In the present study, polyol coprecipitation was used for the synthesis of cerium oxide nanoproducts. The chelating agent reduced the kinetics of nucleation growth, which is important to control the particle size, shape, and aggregation at low temperatures. Furthermore, noble metals decreased the surface area because of partial pore blocking that enhanced $CeO_2$ crystallization. The main concern is to encapsulate the precious metals in the host matrix that may result in inefficient utilization of these metals. In this catalyst, the encapsulation structure may generate strong or even maximal metal–ceria interactions, weakening the surface Ce–O bonds and forming more reactive oxygen species. On the basis of enhanced component interaction, it seems promising to prepare excellent low-temperature oxidation catalysts by one-step coprecipitation.

Here is discussed the possible correlation between silver dispersion and the impact on optical, thermal, electrical, and catalytic activity of cerium oxide nanoparticles. Special emphasis was placed upon the optoelectronic and crystal structural behavior of nanoparticles and the oxidation–reduction character of various silver concentration-doped cerium

oxide nanoparticles. The structural, morphological, thermal, and optical properties of silver ions doped into cerium oxide nanoparticles were characterized in detail.

## Experimental

### Materials

$Ce(NO_3)_3 \cdot 6H2O$ (99.99%, BDH, England), $AgNO_3$ (E-Merck, Germany), ethylene glycol, absolute ethanol, and ammonium hydroxide were used as preparatory materials without any further purification. Double-distilled water was prepared using a Milli-Q system (Millipore, Bedford, MA, USA).

### Synthesis

For the preparation of silver ion-doped cerium oxide nanoparticles, 0.2 M cerium nitrate hexahydrate and 0.2 M silver nitrate (the total cation concentration was 1.0 mol, with molar ratios of dopant cation ratios $Ag^{+}$ to $Ce^{3+}$ of 0.01:0.99, 0.03:0.97, and 0.07:0.93) were dissolved separately in 50 ml of ethylene glycol and heated to 80°C. The separately dissolved silver nitrate in ethylene glycol was mixed slowly at 80°C with stirring to obtain a homogenous mixture and heated to reflux for approximately 5 h. The minimum concentration of $NH_4OH$ was added to cause precipitation. The product was isolated with a centrifuge, washed with distilled water to remove unreacted reactants, and dried at 100°C to obtain a fine powder.

X-ray diffraction was performed with a Rigaku-Dmax 2500 diffractometer equipped with copper $K_\alpha$ excitation at 1.54056 Å. A field emission transmission electron microscope equipped with an energy-dispersive X-ray spectrometer (JEM-2100 F, JEOL, Japan) was operated at an accelerating voltage of 200 kV to characterize the morphology and dopant elemental analysis. Thermogravimetric analysis (Mettler Toledo AG, Analytical CH-8603, Schwerzenbach, Switzerland), infrared spectroscopy (PerkinElmer 580B) from 400 to 4000 $cm^{-1}$, and ultraviolet–visible spectroscopy (PerkinElmer Lambda-40) from 200 to 600 nm were used for characterization. The hydrogen temperature program reduction was analyzed by a Thermo-Finnigan TPDRO 1100 with a thermal conductivity detector.

## Results and discussion

X-ray diffraction was used to determine the phase purity, crystal structure, and crystallinity of the silver ion-doped cerium oxide. The diffractograms contain all characteristic peaks that resemble to those of the pure cubic fluorite phase (space group: *Fm*3*m*) for cerium oxide as identified using the standard data JCPDS 78–0694, which is in accord with previously published reports (Deshpande et al. 2005; Wang, Quan, and Lin 2007; Katelnikovas et al. 2008). No other reflection planes corresponding to the secondary part of Ce-based contaminations were observed. The X-ray diffraction results suggest that the nanoparticles have the pure fluorite-type structure. The width of reflection planes were broadened, perhaps due to the low crystalline nature of these materials.

Doping of transition metals into cerium oxide was reported in our previous work to enhance the electrochemical properties of transparent semiconductor metal oxides (Ansari

et al. 2009a, 2009b). Here, we have also observed the impact of doping by the broadening of the planes by an increase in the full-width half-maxima that corresponds to the (111) plane and clearly suggests a decrease in the crystallinity upon silver doping in cerium oxide. The diffraction peaks were slightly shifted to higher angles by X-ray diffraction suggesting a reduction of the unit cell volume. The values of lattice constants for the silver ion-doped cerium oxide nanoparticles for $x$ values of 1.0, 3.0, and 7.0 mol% were 0.5416, 0.5418, and 0.5423 nm, respectively. The average crystallite sizes of the polyol coprecipitate products were 15.1, 14.8, and 13.9 nm for 1.0, 3.0, and 7.0 mol% silver-doped cerium oxide nanoparticles, respectively, according to the standard Scherrer's formula.

After doping with silver ions, the grain size decreased from 15.1 to 13.9 nm as the degree of silver doping is increased. In addition, the $d$-spacing values and lattice parameters of the doped cerium oxide nanoparticles also decreased with an increase in silver doping perhaps due to the replacement of large $Ce^{4+}$ ions (101 pm) by small $Ag^{+}$ ions (67 pm). However, the fluorite structure of cerium oxide crystallized with the $Ce^{4+}$ cation surrounded by eight equivalent $O^{2-}$ ions forming the corners of cube (Deshpande et al. 2005), with each $O^{2-}$ coordinated to four $Ce^{4+}$ due to the interstitial substitution of $Ce^{4+}$ by $Ag^{1+}$ on the created oxygen vacancy. This process causes a change in the Ce–O bond length and a decrease in the lattice constant and crystal size. Moreover, an increase in $Ag^{1+}$ concentration may decrease the coordination number of $Ce^{4+}$ to $O^{2-}$ from eight to seven and introduce $Ce^{3+}$ ions on the crystal lattice and create $O_2$ vacancies and further decrease the crystallite size. These results are in good agreement with the literature reports (Deshpande et al. 2005; Cai et al. 2014; Zhang et al. 2015). Other researchers observed that the lattice parameters of cerium oxide nanoparticles were altered as a function of increasing dopant concentrations (Mitrovic et al. 2007; Cai et al. 2014; Zhang et al. 2015).

### *Transmission electron microscopy and energy-dispersive X-ray spectroscopy*

The size and morphology of the silver ion-doped cerium oxide nanoparticles were characterized by transmission electron microscopy. Figure 2 shows the high crystalline nature of silver-doped cerium oxide nanoparticles. The images display cubic nanocrystals with an average particle sizes between 10 and 18 nm, thereby confirming the X-ray diffraction

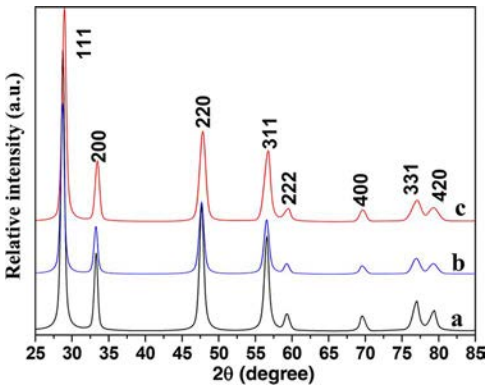


**Figure 1.** X-ray diffraction of (a) 1% Ag:$CeO_2$, (b) 3% Ag:$CeO_2$, and (c) 7% Ag:$CeO_2$ nanoparticles.

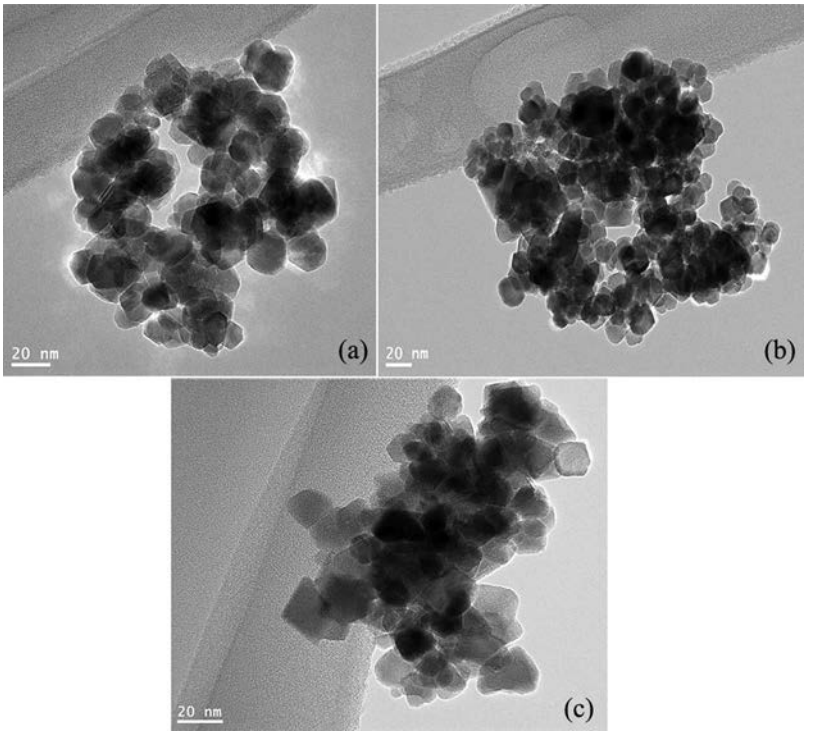


**Figure 2.** Field emission transmission electron microscopy of (a) 1% Ag:$CeO_2$, (b) 3% Ag:$CeO_2$, and (c) 7% Ag:$CeO_2$ nanoparticles.

results. Representative energy-dispersive X-ray spectroscopy confirms the chemical composition of silver-doped cerium oxide nanoparticles and shows the presence of silver, cerium, and oxygen (Figure 3). An enhancement in silver peak is observed showing the increasing concentration of silver ion in the cerium oxide matrix. The C and Cu peaks are from the carbon-coated copper transmission electron microscopy grid. No other impurities were present in the spectra indicating the purity of nanomaterials.

### *Thermogravimetric analysis*

Thermogravimetric analysis of the prepared silver-doped cerium oxide nanoparticles from room temperature to 800°C under nitrogen at 10°C $min^{-1}$ are shown in Figure 4. All prepared nanoparticles displayed thermal stability with similar two-phase decay. A small decrease at 200°C in the thermogravimetric curve was due to the physically adsorbed moisture on the surface of nanopowder. A small mass loss (~3%) was observed from 200 to 800°C due to the loss of surface OH groups or organic groups in various bonding states. In general, two types of surface hydroxyl groups were present: terminal cerium-hydroxyl and association cerium-(hydroxyl)-cerium. The results show that decomposition temperatures of the hydroxyl groups differed because of their surrounding chemical environment. Therefore, a decreased weight loss for hydroxyl groups was observed as a function of temperature. These results are in agreement with X-ray diffraction results. There was no weight loss observed above 800°C.

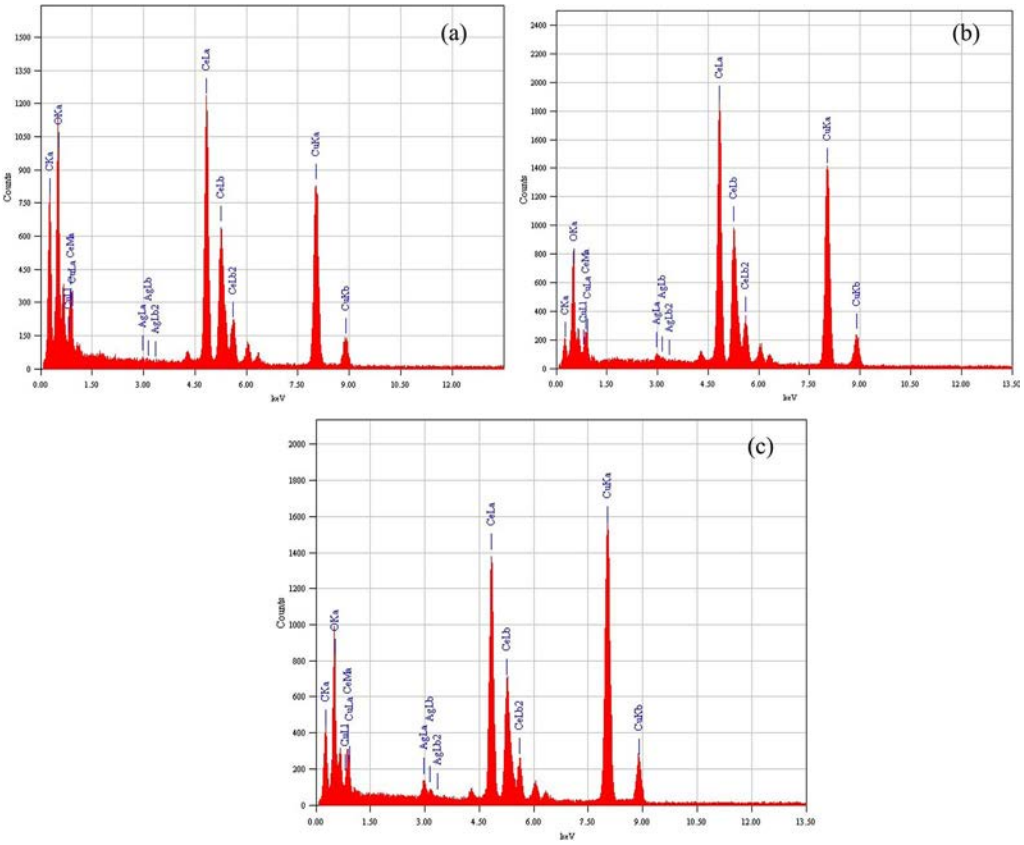


**Figure 3.** Energy-dispersive X-ray analysis of (a) 1% Ag:$CeO_2$, (b) 3% Ag:$CeO_2$, and (c) 7% Ag:$CeO_2$ nanoparticles.

### *Infrared spectroscopy*

Infrared spectroscopy was used from 400 to 4000 $cm^{-1}$ to characterize the surface of silver-doped cerium oxide nanoparticles. Figure 5 shows infrared bands with diminished intensity were present at 3419 $cm^{-1}$ ($\nu$O–H), 1540 $cm^{-1}$ ($\delta$O–H), and 1383 $cm^{-1}$($\rho$O–H) due to $\nu$O–H symmetrical stretching and bending of physically absorbed water on the surface of nanoparticles (Ansari et al. 2008; Ansari, Solanki, and Malhotra 2009; Ansari 2010). The weak intensity peaks demonstrate the low concentration of water that was confirmed by the thermogravimetric analysis. A strong infrared band at 435 $cm^{-1}$ was present due to a phonon band and M–O network (Ansari et al. 2008; Ansari, Solanki, and Malhotra 2009; Ansari et al. 2009a).

### *Ultraviolet–visible spectroscopy and the energy band gap*

The optical responses of silver ion-doped cerium oxide nanoparticles were examined by optical absorption spectra. Figure 6 shows a strong peak due to a charge transfer transition between oxygen (2*p*) to cerium (4*f*), which is the prominent selection rule *f*–*f* transition of $Ce^{4+}$ state (Tsunekawa, Fukuda, and Kasuya 2000). The absorption edge shifted to higher wavelengths with the increasing silver concentrations. However, for 1 mol% silver-doped

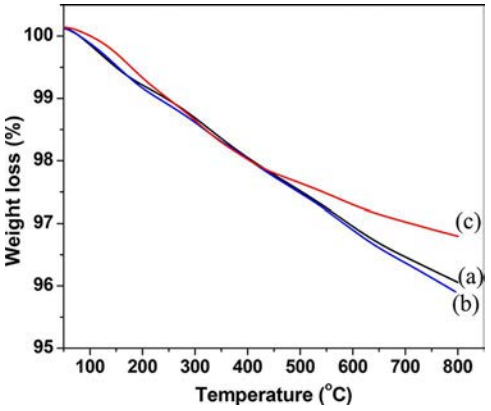


**Figure 4.** Thermogravimetric analysis of (a) 1% Ag:$CeO_2$, (b) 3% Ag:$CeO_2$, and (c) 7% Ag:$CeO_2$ nanoparticles.



cerium oxide, the band was slightly shifted compared to the other two silver-doped cerium oxide nanoparticles. Moreover, no surface plasmon resonance absorbance transition of silver was present in the optical spectra due to small concentrations of silver ions uniformly distributed inside the lattice of cerium oxide (Tsunekawa, Fukuda, and Kasuya 2000; Ansari 2010). We believe that the observed absorption edge is an expected alteration of the crystalline size because cerium oxide is a well-known direct band gap semiconductor. The band gap energy of the silver ion-doped cerium oxide nanocrystals was determined based on reflectance spectra from

$$\alpha h\nu = B(ah\nu - E_g)^{1/2} \tag{1}$$

where $B$ is a constant, $\alpha$ is the optical absorption coefficient, $E_g$ is the direct band gap, and $h\nu$ is the photon energy. The direct band gap was calculated by plotting $(\alpha h\nu)^2$ as a function of $h\nu$ and extrapolating the linear portion of the curve to $x$-axis (Tauc and Menth 1972). Figure 7 shows that the values were 2.04, 1.92, and 1.86 eV for the 1.0, 3.0, and 7.0 mol% silver-doped cerium oxide nanoparticles, respectively. The decreasing trend in the direct band with the increasing silver-doping concentration was due to the presence of extra

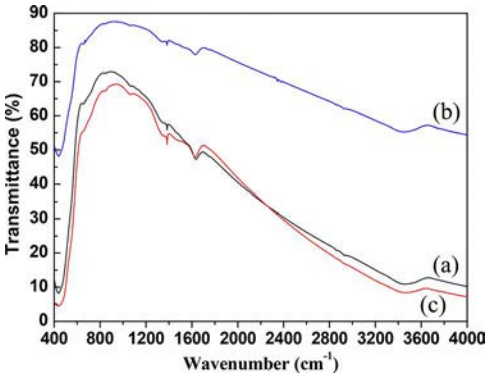


**Figure 5.** Infrared spectra of (a) 1% Ag:$CeO_2$, (b) 3% Ag:$CeO_2$, and (c) 7% Ag:$CeO_2$ nanoparticles.

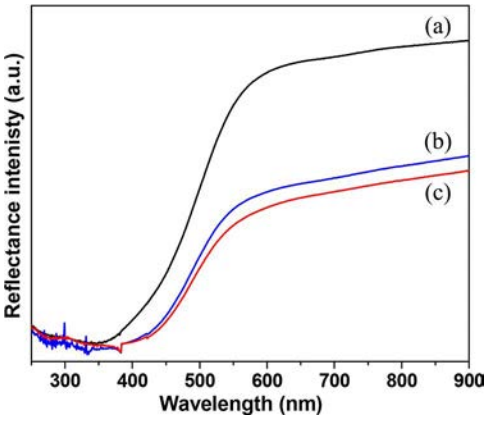


**Figure 6.** Ultraviolet–visible absorption spectra in ethanol of (a) 1% Ag:$CeO_2$, (b) 3% Ag:$CeO_2$, and (c) 7% Ag:$CeO_2$ nanoparticles.



imperfection states within the band gap. The direct band gap represents the energy width of the localized states. Following silver-doping, the extremity of imperfection states is increased, inducing the reduction of direct band gap.

These observed $E_g$ values were in agreement with the literature reports (Zhang et al. 2003; Brito et al. 2010; Dhannia et al. 2010; Ansari, Singh, and Malhotra 2011). The lower value of direct band gap in 7 mol% Ag-doped $CeO_2$ nanoparticles with respect to bulk cerium oxide was caused by quantum size effects (Qu et al. 2013). The observed redshift in the band gap of cerium oxide nanoparticles was observed with the expected blueshift due to quantum confinement. The redshift in the band gap energy may be due to the presence of trivalent cerium ions. The $Ce^{3+}$ ions were generated by the high surface-to-volume ratio of nanocrystals, which enhances the removal of oxygen and promotes the reduction of $Ce^{4+}$ to $Ce^{3+}$. Hence, small concentrations of $Ce^{3+}$ were present

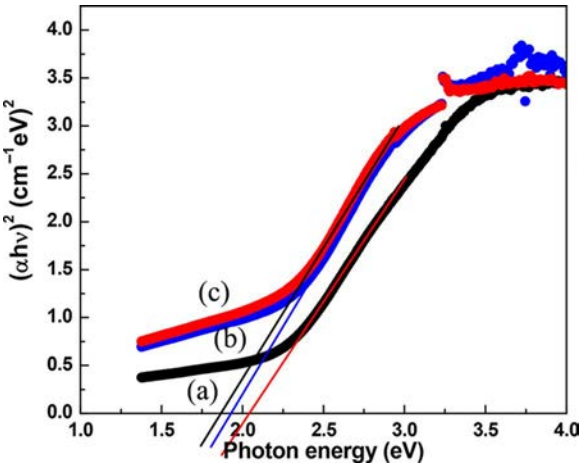


**Figure 7.** Plot of $(\alpha h\nu)^2$ as a function of photon energy of (a) 1% Ag:$CeO_2$, (b) 3% Ag:$CeO_2$, and (c) 7%Ag:$CeO_2$ nanoparticles.

with $Ce^{4+}$ and $Ce^{3+}/Ce^{4+}$ ratio increased with a decrease in the particle size of nanocrystals (Masui et al. 1997; Yin et al. 2002; Deshpande et al. 2005; Wang, Quan, and Lin 2007). The introduction of $Ce^{3+}$ affected the $O_2$ ion position and defects on the external surface of the particles that affected the band gap. For silver dopant concentrations below 7 mol%, it is promising to induce a change of optical absorption edge in cerium oxide nanoparticles to the visible, suggesting that this material may have applications in photocatalysis by sunlight.

## Redox properties

Hydrogen temperature program reduction was performed to examine the impact of silver doping upon the redox behavior of cerium oxide nanoparticles. The temperature program reduction profiles of the silver-doped cerium oxide catalysts are shown in Figure 8 to characterize the influence of silver doping and loading on the redox properties of $CeO_2$ nanoparticles. Two bands are observed in 1 mol% silver-doped $CeO_2$ nanoparticles at 181 and 420°C. The broad band at low temperature is most probably due to the surface reduction at 181°C of $Ce^{4+}$, although contributions from surface carbonates cannot be excluded. The high temperature band is due to bulk reduction of $CeO_2$ nanoparticles.

The high intensity of the first low temperature band reflects the small size of particles. These results are in good agreement with the literature reports (Zhang et al. 2003; Brito et al. 2010; Dhannia et al. 2010; Cai et al. 2014; Zhang et al. 2015). As the concentration of silver increased, the temperature program reduction profile shifted to lower temperature at 148°C with similar intensity for the doublet band. A similar trend was observed for 7 mol% silver-doped $CeO_2$. There is an overall double-intensity band at low temperature with a shift of the second component of doublet to lower temperatures. Moreover, there is a growth and shift to lower temperatures of the bulk band.

Oxygen vacancies may play a decisive role in the surface reactivity and catalytic performance of $CeO_2$ nanoparticles. Here, we expect that the shift of a high-intensity reduction band at low temperatures may be due to the reduction of $Ag^+$ in the surface cerium–oxygen–silver groups, since these are known to be reduced before $Ce^{4+}$(Zhang et al. 2015). However, the substantial broadening and shifting to lower temperatures of the high-temperature bands in the mixed oxides are probably due to easier extraction of

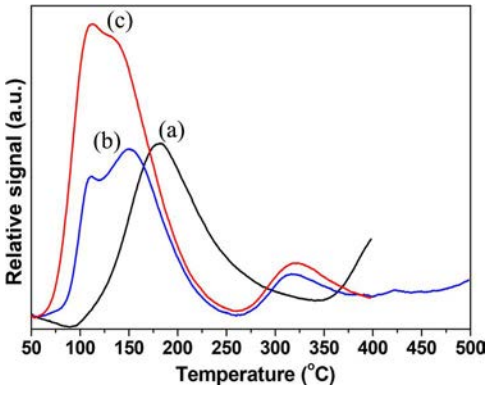


**Figure 8.** Temperature program reduction spectra of (a) 1% Ag:$CeO_2$, (b) 3% Ag:$CeO_2$, and (c) 7% Ag:$CeO_2$ nanoparticles.

oxygen ions from distorted cerium–oxygen–silver groups in the bulk and hindered sintering of the doped nanocrystals (Cai et al. 2014). Literature reports (Zhang et al. 2003; Brito et al. 2010; Dhannia et al. 2010; Cai et al. 2014; Zhang et al. 2015) suggested that the presence of silver weakened the cerium–oxygen bond adjacent to silver and facilitated the reducibility of surface capping $O_2$ of cerium oxide. Therefore, the peaks with maxima at 148 and 112°C, respectively, for 3 and 7 mol% silver-doped cerium oxide samples, may be due to the reduction of surface capping $O_2$ of cerium oxide interacting with silver ions (Cai et al. 2014; Zhang et al. 2015).

The observed double band in 3 and 7 mol% silver-doped cerium oxide may be due to the presence of silver as $Ag^0$ and $Ag^+$ with the reduction peaks at 110 and 111°C. This observation may be due to the elimination of silver oxides or oxygen on the nanodispersed silver ions. The temperature reduction results show that the 7 mol% silver-doped cerium oxide provided exceptional catalytic performance compared to the other materials. The results show that the silver ions stimulated the surface lattice for easy removal of surface oxygen vacancies in cerium oxide lattice and decomposition of hydrogen which greatly facilitates the surface reduction of cerium oxide nanocrystals at low temperatures.

## Conclusion

Silver ion-doped cerium oxide nanoparticles prepared by polyol coprecipitation were characterized by spectroscopic techniques. The results show that the silver ions were homogenously distributed in the cerium oxide lattice. The redox behavior of cerium oxide to convert $Ce^{3+}$ into $Ce^{4+}$ ions was compensated by $O_2$ vacancies, causing a distorted crystal lattice affecting the physiochemical properties of cerium oxide nanoparticles. The influence of silver doping was clearly observed on band gap energies of cerium oxide particles that were modulated by varying the particle size based on quantum confinement effects. The synergistic interaction between silver and cerium oxide was responsible for the reduction of cerium oxide at low temperatures. The 7 mol% doping with silver ions showed higher reducibility at low temperature than the 1 and 3 mol% silver-doped cerium oxide nanoparticles. These observations of silver-doped cerium oxide may have applications in catalysis and other technologies.

## Funding

The authors would like to extend their sincere appreciation to the Deanship of Scientific Research at King Saud University for funding this Research group No. RG 1435-004.

## ORCID

A. A. Ansari http://orcid.org/0000-0002-8708-6673

## References

Ansari, A. A. 2010. Optical and structural properties of sol–gel derived nanostructured $CeO_2$ film. *Journal Semiconductors* 31:053001-5. doi:10.1088/1674-4926/31/5/053001

Ansari, A. A., A. Kaushik, P. R. Solanki, and B. D. Malhotra. 2008. Sol–gel derived nanoporous cerium oxide film for application to cholesterol biosensor. *Electrochemistry Communications* 10:1246–49. doi:10.1016/j.elecom.2008.06.003

Ansari, A. A., S. P. Singh, and B. D. Malhotra. 2011. Optical and structural properties of nanostructured $CeO_2$:$Tb^{3+}$ film. *Journal Alloy & Compounds* 509:262–65. doi:10.1016/j.jallcom.2010.07.009

Ansari, A. A., P. R. Solanki, and B. D. Malhotra. 2008. Sol-gel derived nanostructured cerium oxide film for glucose sensor. *Applied Physics Letters* 93:263901–903. doi:10.1063/1.2953686

Ansari, A. A., P. R. Solanki, and B. D. Malhotra. 2009. Hydrogen peroxide sensor based on horseradish peroxidase immobilized nanostructured cerium oxide film. *Journal Biotechnology* 142:179–84. doi:10.1016/j.jbiotec.2009.04.005

Ansari, A. A., G. Sumana, R. Khan, and B. D. Malhotra. 2009a. Polyaniline-cerium oxide nanocomposite for hydrogen peroxide sensor. *Journal of Nanoscience and Nanotechnology* 9:4679–86. doi:10.1166/jnn.2009.1085

Ansari, A. A., G. Sumana, M. K. Pandey, and B. D. Malhotra. 2009b. Sol-gel-derived titanium oxide–cerium oxide biocompatible nanocomposite film for urea sensor. *Journal Materials Research* 24:1667–74. doi:10.1557/jmr.2009.0212

Ayastuy, J. L., E. F. Puertas, M. P. G. Marcos, and M. A. G. Ortiz. 2012. Transition metal promoters in $CuO/CeO_2$ catalysts for CO removal from hydrogen streams. *International Journal Hydrogen Energies* 37:7385–97. doi:10.1016/j.ijhydene.2012.02.007

Banerjee, S., P. S. Devi, D. Topwal, S. Mandal, and K. Menon. 2007. Enhanced ionic conductivity in $Ce_{0.8}Sm_{0.2}O_{1.9}$: Unique effect of calcium co-doping. *Advanced Functional Materials* 17:2847–54. doi:10.1002/adfm.200600890

Brito, P. C. A., D. A. A. Santos, J. G. S. Duque, and M. A. Macedo. 2010. Structural and magnetic study of Fe-doped $CeO_2$. *Physica B* 405:1821–25. doi:10.1016/j.physb.2010.01.054

Cai, S., D. Zhang, L. Zhang, L. Huang, H. Li, R. Gao, L. Shi, and J. Zhang. 2014. Comparative study of 3D ordered macroporous $Ce_{0.75}Zr_{0.2}M_{0.05}O_{2-\delta}$ (M=Fe, Cu, Mn, Co) for selective catalytic reduction of NO with $NH_3$. *Catalysis Science Technology* 4:93–101. doi:10.1039/c3cy00398a

Chang, S., M. Li, Q. Hua, L. Zhang, Y. Ma, B. Ye, and W. Huang. 2012. Shape-dependent interplay between oxygen vacancies and silver–$CeO_2$ interaction in silver/$CeO_2$ catalysts and their influence on the catalytic activity. *Journal Catalysis* 293:195–204. doi:10.1016/j.jcat.2012.06.025

Chen, J., S. Patil, S. Seal, and J. F. McGinnis. 2006. Rare earth nanoparticles prevent retinal degeneration induced by intracellular peroxides. *Nature Nanotechnology* 1:142. doi:10.1038/nnano.2006.91

Deshpande, S., S. Patil, S. V. N. T. Kuchibhatla, and S. Seal. 2005. Size dependency variation in lattice parameter and valency states in nanocrystalline cerium oxide. *Applied Physics Letters* 87:133113. doi:10.1063/1.2061873

Dhannia, T., S. Jayalekshmi, M. C. S. Kumar, T. P. Rao, and A. C. Bose. 2010. Effect of iron doping and annealing on structural and optical properties of cerium oxide nanocrystals. *Journal Physical Chemistry Solids* 71:1020–25. doi:10.1016/j.jpcs.2010.04.011

Katelnikovas, A., T. Justel, D. Uhlich, J. E. Jorgensen, S. Sakirzanovas, and A. Kareiva. 2008. Characterization of cerium-doped yttrium aluminium garnet nanopowders synthesized via sol-gel process. *Chemical Engineering Communications* 195:758–769. doi:10.1080/00986440701691194

Liao, L., H. X. Mai, Q. Yuan, H. B. Lu, J. C. Li, C. Liu, C. H. Yan, Z. X. Shen, and T. Yu. 2008. Single $CeO_2$ nanowire gas sensor supported with Pt nanocrystals: Gas sensitivity, surface bond states, and chemical mechanism. *Journal Physical Chemistry C* 112:9061–65. doi:10.1021/jp7117778

Masui, T., K. Fujiwara, K. Machida, and G. Adachi. 1997. Characterization of cerium(IV) oxide ultrafine particles prepared using reversed micelles. *Chemistry Materials* 9:2197–204. doi:10.1021/cm970359v

Mitrovic, Z. D. D., M. Radovic, M. Scepanovic, M. G. Brojcin, Z. V. Popovic, B. Matovic, and S. Boskovic. 2007. Temperature-dependent Raman study of $Ce_{0.75}Nd_{0.25}O_{2-\delta}$ nanocrystals. *Applied Physics Letters* 91:203118. doi:10.1063/1.2815928

NaeemUllah, K., T. G. Kazi, H. I. Afridi, F. Shah, S. S. Arain, A. H. Panhwar, S. A. Arain, and M. B. Arain. 2014. Development of green miniaturize dispersive ionic liquid nano-emulsion method for

preconcentration of cadmium from canal and waste water samples prior to couple with graphite furnace atomic absorption spectrometry. *Analytical Method* 6 (17):6909–915. doi:10.1039/c4ay01280a

Qu, Z., F. Yu, X. Zhang, Y. Wang, and J. Gao. 2013. Support effects on the structure and catalytic activity of mesoporous Silver/$CeO_2$ catalysts for CO oxidation. *Chemical Engineering Journal* 229:522–32. doi:10.1016/j.cej.2013.06.061

Robert, C. L., J. W. Long, K. A. Pettigrew, R. M. Stroud, and D. R. Rolison. 2007. Ionic nanowires at 600°C: Using nanoarchitecture to optimize electrical transport in nanocrystalline gadolinium-doped ceria. *Advanced Materials* 19:1734–39. doi:10.1002/adma.200601840

Si, R., Y. W. Zhang, L. P. You, and C. H. Yan. 2005. Rare-earth oxide nanopolyhedra, nanoplates, and nanodisks. *Angewandte Chemie International Edition* 44:3256–60. doi:10.1002/anie.200462573

Souza, E. C. C., and E. N. S. Muccillo. 2009. Effect of solvent on physical properties of samaria-doped ceria prepared by homogeneous precipitation. *Journal Alloys Compounds* 473:560–66. doi:10.1016/j.jallcom.2008.06.027

Tauc, J., and A. Menth. 1972. States in the gap. *Journal of Non-Crystalline Solids* 8/9:569–85.

Tsunekawa, S., T. Fukuda, and A. Kasuya. 2000. Blue shift in ultraviolet absorption spectra of monodisperse $CeO_{2-x}$ nanoparticles. *Journal of Applied Physics* 87:1318–21. doi:10.1063/1.372016

Wadhwa, S. K., M. Tuzen, T. G. Kazi, and M. Soylak. 2013. Graphite furnace atomic absorption spectrometric detection of vanadium in water and food samples after solid phase extraction on multiwalled carbon nanotubes. *Talanta* 116:205–209. doi:10.1016/j.talanta.2013.05.020

Wang, Z., Z. Quan, and J. Lin. 2007. Remarkable changes in the optical properties of $CeO_2$ nanocrystals induced by lanthanide ions doping. *Inorganic Chemistry* 46:5237–42. doi:10.1021/ic0701256

Yin, L. X., Y. Wang, G. Pang, Y. Koltypin, and A. Gedanken. 2002. Sonochemical Synthesis of cerium oxide nanoparticles—Effect of additives and quantum size effect. *Journal of Colloid Interface Science* 246:78–84. doi:10.1006/jcis.2001.8047

Yu, T., J. Joo, Y. I. Park, and T. Hyeon. 2005. Large-scale nonhydrolytic sol–gel synthesis of uniform-sized ceria nanocrystals with spherical, wire, and tadpole shapes. *Angewandte Chemie International Edition* 44:7411–14. doi:10.1002/anie.200500992

Yu, T., J. Zeng, B. Lim, and Y. Xia. 2010. Aqueous-phase synthesis of Pt/$CeO_2$ hybrid nanostructures and their catalytic properties. *Advanced Materials* 22:5188–92. doi:10.1002/adma.201002763

Zhang, J., J. Guo, W. Liu, S. Wang, A. Xie, X. Liu, J. Wang, and Y. Yang. 2015. Facile preparation of $Mn^{+}$-doped (M=Cu, Co, Ni, Mn) hierarchically mesoporous $CeO_2$ nanoparticles with enhanced catalytic activity for CO oxidation. *European Journal Inorganic Chemistry* 2015:969–77. doi:10.1002/ejic.201403078

Zhang, Y. W., R. Si, C. S. Liao, C. H. Yan, C. X. Xiao, and Y. Kou. 2003. Facile alcohothermal synthesis, size-dependent ultraviolet absorption, and enhanced CO conversion activity of ceria nanocrystals. *Journal of Physical Chemistry B* 107:10159–67. doi:10.1021/jp034981o